Atomistic Origin of the Thermally Driven Softening of Raman Optical Phonons in Group III Nitrides

M. X. Gu,[†] L. K. Pan,[‡] T. C. Au Yeung,[†] B. K. Tay,[†] and Chang Q. Sun*,[†]

School of Electrical and Electronic Engineering, Nanyang Technological University, Singapore 639798, and Engineering Research Center for Nanophotonics & Advanced Instrument, Ministry of Education, East China Normal University, Shanghai, China 20006

Received: April 6, 2007; In Final Form: May 23, 2007

It has long been puzzling regarding the physical origin of the thermally induced red-shift of Raman optical phonons in group III nitride crystals despite some possible mechanisms such as phonon decay, thermal expansion, interfacial effects, or their combinations. Here we show that an extension of the recent approach [Sun, C. Q.; Pan, L. K.; Li, C. M.; Li, S. *Phys. Rev. B* **2005**, *72*, 134301] to the functional dependence of the frequency of Raman optical modes on the atomic bonding identities (bond length, bond strength, and atomic coordination numbers) to the temperature domain has enabled us to gain a simple solution with improved understanding of the thermally induced red-shift of Raman optical phonons. Reproduction of the measured temperature dependence of the Raman shift of AlN, GaN, and InN reveals that the thermally driven red-shift arises simply from bond vibration and bond expansion, together with derived information about the *mode* cohesive energy.

I. Introduction

The vibronic behavior of atoms in a specimen such as group III nitrides (GaN, AlN, and InN) is not only of fundamental significance to processes such as electron−phonon coupling, phonon−photon interaction, phonon transport, and thermal conductivity, but also of technical importance to practical applications in fields such as short wavelength light emitting, high temperature, high frequency, high power electronic, and thermal devices.[1−4] Generally, a red-shift of Raman optical phonons happens when the temperature of measurement is raised, such as in the case of GaN,[5−8] AlN,[9,10] and InN.[11] Similar trends of the temperature dependence of Raman shift have also been observed from some other materials.[12−18] However, the mechanisms for the observations are still puzzling with the following possible models:[5−18]

$$\frac{\Delta\omega(T)}{\omega_0}=\frac{\omega(T)-\omega_0}{\omega_0}=\begin{cases}\Delta_1(T) & \text{(Balkanski et al.)}\\ \Delta_1(T)+\Delta_2(T) & \text{(Menendez et al.)}\\ \Delta_1(T)+\Delta_2(T)+\Delta_3(T) & \text{(Qian et al.)}\\ \Delta_4(T) & \text{(Liu et al.)}\end{cases} \quad (1)$$

with

$$\Delta_1(T)=\mathrm{A}_1\left\{1+\frac{1}{e^x-1}\right\}+A_2\left\{1+\frac{1}{e^y-1}+\frac{1}{(e^y-1)^2}\right\} \quad \text{(Anharmonic-phonon-decay)}$$

$$\Delta_2(T)=\exp[-3\gamma_i\int_0^T\alpha(t)\,\mathrm{d}t]-1 \quad \text{(Thermal-expansion)}$$

$$\Delta_3(T)=2\left(a-b\frac{C_{13}}{C_{33}}\right)\times\left[(1+\epsilon_g)\frac{1+\int_{T_g}^T\alpha_s(t)\,\mathrm{d}t}{1+\int_{T_g}^T\alpha(t)\,\mathrm{d}t}-1\right] \quad \text{(Interface-contribution)}$$

$$\Delta_4(T)=\frac{B_1}{e^{B_2\hbar\omega(T_0)/k_BT}-1} \quad \text{(Simplified phonon decay)} \quad (2)$$

where ω_0 is the specific Raman phonon frequency measured at reference temperature 0 K, T is the temperature of measurement, and t is the integrand. $x=\hbar\omega_0/2k_BT$ and $y=2x/3$ (k_B is Boltzmans constant) correspond to the third and the forth order of phonon decay, respectively. The constants A_1, A_2, B_1, and B_2 are feely adjustable parameters needing clear physical indications. The other parameters in eq 2 are physically meaningful and experimentally obtainable. For example, γ_i is the mode Grüneisen parameter and the value of γ_i varies from mode to mode. $\alpha(T)$ is the coefficient of thermal expansion of the specimen and $\alpha_s(T)$ is the coefficient of thermal expansion of the substrate when the interface interaction is involved. ϵ_g is the residual strain in the sample at the growth temperature T_g. C_{13}/C_{33} is the elastic constant ratio of the 13 and 33 elements in the elastic tensor. The parameters a and b in Δ_3 are phonon deformation potentials.[11,19]

* Address correspondence to this author. E-mail: ecqsun@ntu.edu.sg.
[†] Nanyang Technological University.
[‡] East China Normal University.

10.1021/jp0727087 CCC: $37.00
Published on Web 08/18/2007

The models given in eq 1 represent that the phonon red-shift may arise from anharmonic phonon decay, thermal expansion, the interface interaction, or the combination of these factors. Except for the terms of phonon decay, the additional terms originate from the change of macroscopic properties with temperature. The red-shift of the optical modes represented by the A_1-related term in Δ_1 was first assumed arising from the decay of one optical phonon into two acoustic phonons of the same frequency but opposite momentum upon the sample being excited by the incident photons.[20] The phonon decay has been extended to the higher fourth order represented by the A_2-related term in Δ_1.[21] Later, the effect of thermal expansion in Δ_2 was considered.[22] Some works have shown that good reproduction of the measured T dependence of the red-shift of Raman optical phonon could be reached without considering the effect of thermal expansion.[13,17,18,20,23,24] However, some calculations indicated that thermal expansion also played a certain non-negligible role in the T-induced red-shift of the Raman frequency.[7,9,15,25−27] Sometimes the temperature-dependent strain induced by lattice and thermal mismatch between the specimen and the substrate became essential when the interface effect was considered, and this is represented by Δ_3.[4,5,11] From the quantum mechanical point of view, the T-induced Raman red-shift can be fitted to a Bose−Einstein population as indicated by Δ_4.[6,18] On the other hand, the first principle ab initio calculations have also been conducted to calculate some of the individual terms in eq 2 and then added up to examine the factors dominating the temperature dependence[28−30] on the Raman modes.

In fact, the T-induced Raman red-shift can be numerically reproduced by using all the models in eq 2. Unfortunately, no relationship has been established between the T-induced Raman shift and the atomistic parameters, i.e., the bonding identities (bond length, bond strength, and bond order). Here we show that an extension of the recent approach for the size-induced Raman shift of nanostructures[31,32] to the temperature domain could lead to an immediate solution with one fitting parameter termed as *mode* cohesive energy. Reproduction of the observations revealed that the red-shift arises simply from thermally induced bond vibration and bond expansion.

II. Principle

Recent progress[31,33] showed that it is possible to connect the macro properties of a specimen to its atomistic parameters by developing the functional dependence of the detectable quantities to the bonding identities and the response of these bonding identities to the external stimulus such as coordination environment,[33] temperature (vibration and expansion),[34,35] pressure, etc. For instance, coordination number reduction causes the remaining bonds of the under-coordinated atoms to be shorter and stronger; the rise in temperature has an opposite effect on the length and strength of all the bonds in the specimen through the thermal vibration. From these perspectives, we have developed the functional dependence of the frequency of Raman optical phonons on the atomic coordination, z, bond length, d, and the bond energy, E_b, at $T \approx 0$ K[31,32]

$$\omega(0) \propto \frac{z}{d}\left[\frac{E_b(0)}{\mu}\right]^{1/2} \tag{3}$$

where μ is the reduced mass of the bonding atoms. $E_b(0)$ is the *mode* bonding energy (as will be elaborated shortly) at 0 K for a specific bond. Equation 3 shows that the macroscopically measurable Raman frequency is directly related to the coordination number z, the bond length d, the square root of *mode* cohesive energy $E_b(0)$, and the reduced mass of the bonding atoms μ. By using the core−shell configuration for nanostructures, eq 3 has allowed us to reproduce the size-dependent red-shift of the Raman optical frequency with derived information on the vibration frequency of an isolated dimer in InP, CeO2, SnO2, CdS, and Si nanostructures at temperatures far below the melting point.[31]

Equation 3 is valid at a very low temperature of measurement ($T \ll \theta_D$, θ_D is Debye temperature). If the temperature effect is considered, i.e., by considering the temperature effect on bonding identities, we can extend eq 3 to the temperature domain,

$$\omega(T) \propto \frac{z}{d}\left[\frac{E_b(T)}{\mu}\right]^{1/2} \tag{4}$$

where[34]

$$\begin{cases} E_b(T) = E_b(0) - \int_0^T \eta_1(t)\,\mathrm{d}t \\ d(T) = d_0[1 + \int_0^T \alpha(t)\,\mathrm{d}t \end{cases} \tag{5}$$

where $\eta_1(t)$ is the specific heat per bond, which follows the specific heat of Debye approximation and reaches a constant value at high temperature. $\alpha(T)$ remains the temperature-dependent thermal expansion coefficient. d_0 is the bond length at 0 K. The integration $\int_0^T \eta_1(t)\mathrm{d}t$ represents the thermal vibration energy. Combining eqs 4 and 5 leads to

$$\omega(T) \propto \frac{z[(E_b(0) - \int_0^T \eta_1(t)\,\mathrm{d}t)/\mu]^{1/2}}{d(1 + \int_0^T \alpha(t)\,\mathrm{d}t)} \tag{6}$$

or, the relative frequency ω measured at temperature T to that measured at the 0 K,

$$\frac{\omega(T)}{\omega_0} = \begin{cases} (1 + \int_0^T \alpha(t)\,\mathrm{d}t)^{-1}\left(1 - \dfrac{\int_0^T \eta_1(t)\,\mathrm{d}t}{E_b(0)}\right)^{1/2}, (T_0 = 0; T < \theta_D) \\ (1 + \int_0^T \alpha(t)\,\mathrm{d}t)^{-1}\left(1 - \dfrac{\eta_1 T}{E_b(0)}\right)^{1/2}, (T_0 = 0; T > \theta_D) \end{cases} \tag{7}$$

with $E_b(0)$, the *mode* cohesive energy, being the only fitting parameter for a specific mode. The *mode* cohesive energy is a certain portion of atomic bonding energy.

The specific heat per bond, $\eta_1(T)$, and the integration of $\eta_1(t)$ from 0 K to T or the conventionally termed specific internal energy per bond, $u(T)$, follow the relations

$$\eta_1(t/\theta_D) = \frac{c_v(T/\theta_D)}{z} = \frac{9R}{z}\left(\frac{T}{\theta_D}\right)^3 \int_0^{\theta_D/T} \frac{x^4 \exp(x)}{e^x - 1)^2}\,\mathrm{d}x$$

$$u(T/\theta_D) = \frac{U(T/\theta_D)}{z} = \frac{\int_0^T c_v(t)\,\mathrm{d}t}{z} \frac{9R}{z}\left(\frac{T}{\theta_D}\right)^3 \int_0^{\theta_D/T} \frac{x^3\,\mathrm{d}x}{e^x - 1}$$

When the measuring temperature T is higher than θ_D, the specific heat c_v approaches a constant value of $3R$ (R is the idea gas constant) according to Debye's approximation.

III. Results and Discussion

The calculation was conducted with eq 7. The parameters of melting temperature, T_m, Debye temperature, θ_D, and the

TABLE 1: List of Input Data and Derived Mode Cohesive Energy for Eq 7[a]

	T_m (K)	θ_D (K)	α (ref)	Raman mode	ω_0 (cm^{-1})	$E_b(0)$ (eV)	Σ (×10^{-4})
AlN	3273	1150	$\alpha_c = -0.93 + (9.1 \times 10^{-2})T - (2.4 \times 10^{-6})$ $\alpha_c = -0.73 + (7.5 \times 10^{-2})T - (2.1 \times 10^{-6})$ ref 36	E_2(high)	658.6	1.13	0.94
				A_1(LO)	892.6	1.21	1.54
				A_1(TO)	613	0.71	1.74
				E_1(LO)	914.7	1.31	1.52
				E_1(TO)	671.6	1.19	1.04
GaN	2773	600	$\alpha_v = \sum_{i=1}^{n} X_i[(\theta_i/T)^2 \exp(\theta_i/T)]/[\exp(\theta_i/T) - 1]^2$ X_i and θ_i are fitting parameters in ref 40	E_2(high)	570.2	1.44	0.57
				A_1(LO)	738	0.97	1.20
				A_1(TO)	534	1.26	1.28
				E_1(LO)	745	0.95	0.68
				E_1(TO)	561.2	1.59	1.12
InN	1373	600	$\alpha_a = 2.134 + 0.00608T$ $\alpha_c = 2.165 + 0.00260T$ ref 37	E_2(high)	495.1	0.76	1.15
				A_1(LO)	595.8	0.50	0.92

[a] Melting temperature (T_m), Debye temperature (θ_D), and the temperature dependent thermal expansion coefficient (α(T)). The intrinsic Raman frequency at ω_0 is extrapolated from experimental data to 0 K. The fitting results, that is the *mode* cohesive energy at 0 K, $E_b(0)$, of various Raman active modes for AlN and GaN and InN are given in the last second columns. The last column provides the standard deviation between experimental data and our theoretical calculations.

T-dependent thermal expansion coefficient, α(T), are taken as the known data for input as tabulated in Table 1. For cubic crystals the thermal expansion coefficient α is isotropic. However, for noncubic solids such as hexagonal structured group III nitrides discussed here, α is anisotropic. The principal values of α for these hexagonal structures are those parallel and perpendicular to the c-axis, which are denoted as α_c and α_a, respectively. To simplify the analysis, the linear thermal expansion coefficient α is the directionally averaged value, expressed as $\alpha = (2\alpha_a + \alpha_c)/3$.[36,37] The thermal expansion coefficients for AlN in Table 1 are obtained from ref 36 by fitting the experimental data with the reference lattice constants a_0 and c_0 taken at 77 K. The overall thermal expansion coefficients for AlN and InN are from refs 36 and 37. The intrinsic phonon frequencies ω_{0i} (where i refers to different optical Raman modes) are extrapolated from experimental observations to 0 K.

First, the calculation of the frequency shift in the Raman spectrum was conducted at $T > \theta_D$. Since the thermal expansion coefficient α is normally in a range of 10^{-6} K^{-1}, $1 + \int_0^{T_m} \alpha(t)dt \leq 1 + 0.05$. It is reasonable to ignore the thermal expansion for the first order approximation for $T > \theta_D$. Hence, eq 7 can be simplified as

$$\frac{\omega(T)}{\omega_0} = (1 + \int_0^T \alpha(t)\,dt)^{-1}\left(1 - \frac{\eta_1 T}{E_b(0)}\right)^{1/2} \approx (1 + \int_0^T \alpha(t)\,dt)^{-1}\left(1 - \frac{1}{2}\frac{\eta_1 T}{E_b(0)}\right)^{\alpha T \ll 1} \approx 1 - B \times T \quad (8)$$

$$B \approx 1/2 \times \eta_1/E_b(0)$$

which leads to the linear temperature dependence of the optical Raman frequency at sufficiently high temperature. Such a linear approximation at high temperature agrees well with experimental observations, from which the experimental slope B_{exp} can be easily determined by fitting to the linear Raman frequency shift versus T curve at the high-temperature range. By the relation of $B_{exp} \cong {}^1/_2\eta_1/E_b(0)$ with $\eta_1 \equiv 3R/z$ ($T > \theta_D$), the *mode* cohesive energy $E_b(0)$ can be estimated. The derived $E_b(0)$ used as an initial guess can be further refined by carefully fitting the experimental data at the whole temperature range (especially at the low-temperature range) by including the contribution of lattice thermal expansion. Results are listed in Table 1 with given standard deviations.

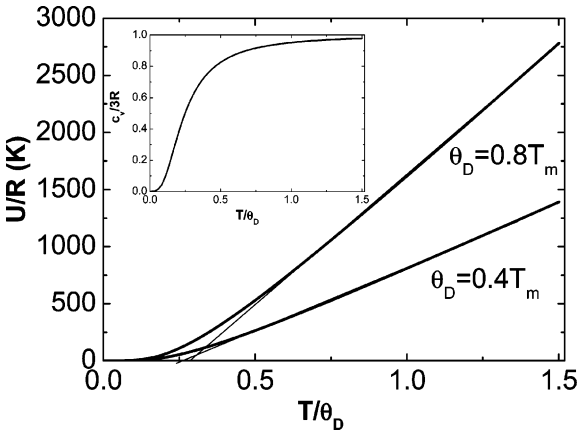

Figure 1. Illustration of the temperature dependence of the reduced specific heat (inset) and its integration with respect to temperature (or the specific internal energy $U(T/\theta_D)$). The melting temperature is chosen to be 1000 K for illustration purposes. For consideration of a single bond, one has to divide the values by the atomic coordination number (CN) z. The $c_v(T/\theta_D)$ and $U(T/\theta_D)$ are sensitive to the Debye temperature.

Figure 1 illustrates the temperature dependence of the reduced specific heat c_v (in units of gas constant R) and its integration with respect to temperature T (or the termed specific internal energy), $U(T/\theta_D)$. For a single bond, one has to divide the values by the atomic coordination number z (in the current discussion, $z = 4$ since each atom has four nearest neighboring atoms). At high T, especially when $T > \theta_D$, the integration of the specific heat or the specific internal energy depends linearly on T as shown in Figure 1. Hence the approximation in eq 8 is reasonable. At low temperatures, on the other hand, the integration shows a nonlinear relationship with respect to the temperature in a T^4 form. The range of nonlinearity depends highly on the Debye temperature θ_D, which can be seen from $U(T/\theta_D)$ in Figure 1. From eqs 7 and 8, it can be seen that the Debye temperature θ_D determines the width of the shoulder and the $E_b(0)$ determines the slope of the curve at high temperature.

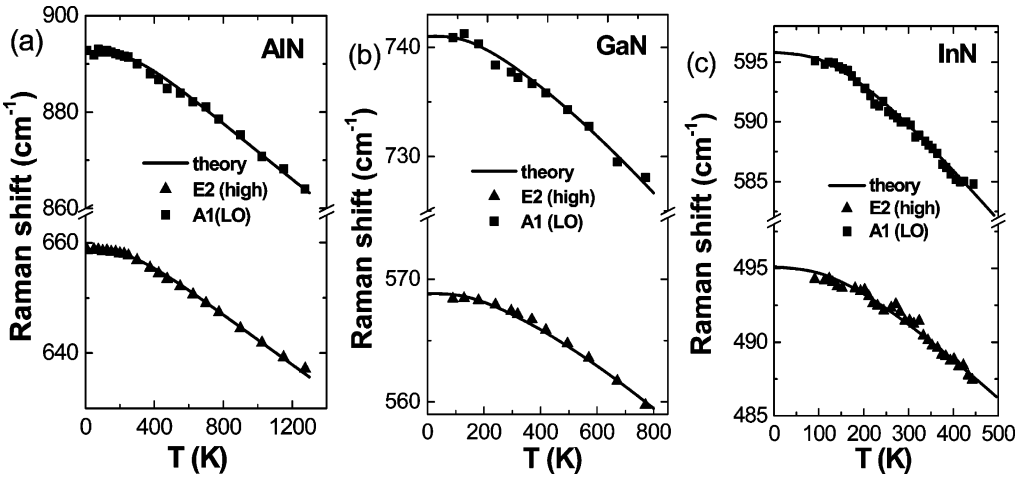

Figure 2. Comparison of the predictions to the measured *T*-dependent optical frequency shift in the Raman spectrum of the A_1 (LO) and the E2 modes for (a) AlN [ref 9], (b) GaN [ref 5], and (c) InN [ref 11] specimens. Extrapolated intrinsic phonon frequency ω_0 and *mode* cohesive energies $E_b(0)$ for various modes are given in Table 1.

Figure 2 shows the agreement between theory and measurement of the typical Raman shifts with derived *mode* cohesive energy $E_b(0)$ given in Table 1. The slow decrease of the Raman shift at very low temperatures arises from the small $\int_0^T \eta_1(t)\,dt$ values as the specific heat $\eta_1(T)$ is proportional to T^3 at very low temperatures (see the inset in Figure 1). It is seen that the θ_D of AlN is higher than that of GaN and InN, and hence the linearity of the optical frequency shift in the Raman spectrum for AlN extends to higher temperature. On the other hand, the $E_b(0)$ for the longitudinal modes A_1(LO) and E_1(LO) of AlN is greater than that of GaN; however, for transverse modes, GaN shows an opposite order, which may arise from different bond strengths in the nitrides. Thus, we have demonstrated that without involving any freely adjustable parameters or mechanisms of phonon decay or the interface interaction, we can reproduce the observations exceedingly well. Interface effect may come into play for ultrathin films, which only modifies the accuracy of the *mode* cohesive energy.

As discussed earlier, the *mode* cohesive energy is different from the bond energy, but they are inter-related. In a complex unit cell containing two atoms, there is one bond between the two atoms. For each bond, there are three optical phonon modes, i.e., LO, TO1, and TO2. One value of atomic bonding energy may correspond to three different values of *mode* cohesive energy. Each value of mode cohesive energy is just a portion of the atomic bonding energy but the exact portion is yet to be known. Furthermore, investigation[38] revealed that the eigenvalues of the Schüdinger equation for lattice vibration follow a Fourier series with multiple orders. Considering the high-order contribution in the solutions to the Raman shift and the dipole−dipole perturbation[38] to the vibration that splits the Raman peaks, there should be more than three modes detectable if they are Raman active. On the other hand, the group theory predicts that for the wurtzite group III nitrides structure that contains two N−metal atom pairs per unit cell, there are eight sets of phonon normal modes at the Γ point. They are $2A_1 + 2E_1 + 2B_1 + 2E_2$, but only the first 6 are Raman active, which are A_1(LO), A_1(TO), E_1(LO), E_1(TO), E_2(high), and E_2(low). These six active Raman modes can be observed by different scattering geometries. The E_2(high) and B_1(high) represent respectively the bending and stretching modes of N−N atoms, while the E_2(low) and B_1(low) correspond to the bending and stretching modes of Al−Al, Ga−Ga, or In−In vibration.[39] Therefore, the *mode* cohesive energy obtained from fitting to E_2 modes will give preliminary information about the strength of N−N bonding in different directions. Information about the strength of metal−metal bonding cannot be obtained since the B_1 is Raman inactive. Furthermore, the A_1 and E_1 modes relate to N−metal bonding in the axial and planar directions. Similarly, the *mode* cohesive energy obtained from fitting to experimental data will give relative information about the N−metal bond energy in both directions. Therefore, for a specific value of bond energy there should be more values of *mode* cohesive energies and each of them is just a portion of the unique bond energy. Hence, the $E_b(0)$ values obtained from fitting to A_1(LO), A_1(TO), E_1(LO), and E_1(TO) modes are only part of the bonding energy, and the exact portion is hardly detectable as so far no means has been available to determine the N−N, N−metal, and metal−metal bond energies.

IV. Summary

In summary, we have presented an approach for the atomistic understanding of the physical origin of the thermally induced red-shift of the Raman optical modes by developing the functional dependence of the macroscopically measurable *T*-dependent Raman optical modes on microscopic atomic bonding identities and the response of these bond identities to the temperature change. A simple and straightforward analytical form has been developed from the perspective of bond vibration and bond expansion An exceedingly good match to the measured *T*-dependent Raman shift of AlN, GaN, and InN specimens has led to information about the *mode* cohesive energy for various phonon modes, which is beyond the scope of conventional approaches. The agreement between the calculation and experimental data may demonstrate that the current expression could represent the true situation of the thermally driven optical phonon frequency red-shift in the Raman spectrum. As this exercise is the first attempt to correlate the macroscopically measurable parameters to microscopic atomic bonding identities in the temperature domain, there is still room for improvement. Further discussions of such an approach to other situations are in progress.

References and Notes

(1) Orton, J. W.; Foxon, C. T. *Rep. Prog. Phys.* **1998**, *61*, 1.

(2) Piprek, J.; Nakamura, S. *IEE Proc. J*: *Optoelectron.* **2001**, *149*, *145*.

(3) Jain, S. C.; Willander, M.; Narayan, J.; Overstraeten, R. Van. *J. Appl. Phys.* **2000**, *87*, *965*.
(4) Qian, Z. G.; Shen, W. Z.; Ogawa, H.; Guo, Q. X. *J. Phys.*: *Condens. Matter* **2004**, *16*, R381.
(5) Link, A.; Bitzer, K.; Limmer, W.; Sauer, R.; Kirchner, C.; Schwegler, V.; Kamp, M.; Ebling, D. G.; Benz, K. W. *J. Appl. Phys.* **1999**, *86*, *6256*.
(6) Liu, M. S.; Bursill, L. A.; Prawer, S.; Nugent, K. W.; Tong, Y. Z.; Zhang, G. Y. *Appl. Phys. Lett.* **1999**, *74*, *3125*.
(7) Li, W. S.; Shen, Z. X.; Feng, Z. C.; Chua, S. J. *J. Appl. Phys.* **2000**, *87*, *3332*.
(8) Harima, H. *J. Phys. Condens. Matter* **2002**, *14*, R967.
(9) Kuball, M.; Hayes, J. M.; Shi, Y.; Edgar, J. H.; Prins, A. D.; Uden, N. W. A.; van Dunstan, D. J. *J. Cryst. Growth* **2001**, *231*, 391.
(10) Kazan, M.; Zgheib, Ch.; Moussaed, E.; Masri, P. *Diamond Relat. Mater.* **2006**, *15*, 1169.
(11) Pu, X. D.; Chen, J.; Shen, W. Z.; Ogawa, H.; Guo, Q. X. *J. Appl. Phys.* **2005**, *98*, 033527.
(12) Tanaka, A.; Onari, S.; Arai, T. *Phys. Rev. B* **1992**, *45*, 6587.
(13) Anand, S.; Verma, P.; Jain, K. P.; Abbi, S. C. *Phys. B* **1996**, *226*, 331.
(14) Ursaki, V. V.; Tiginyanu, I. M.; Zalamai, V. V.; Rusu, E. V.; Emelchenko, G. A.; Masalov, V. M.; Samarov, E. N. *Phys. Rev. B* **2004**, *70*, 155204.
(15) Tang, H.; Herman, I. P. *Phys. Rev. B* **1991**, *43*, 2299.
(16) Su, Z.; Sha, J.; Pan, G.; Liu, J.; Yang, D.; Dickinson C.; Zhou, W. *J. Phys. Chem. B* **2006**, *110*, 1229.
(17) Liu, M. S.; Bursill, L. A.; Prawer, S.; Prawer, S. *Phys. Rev. B* **2000**, *61*, 3391.
(18) Cui, J. B.; Amtmann, K.; Ristein, J.; Ley, L. *J. Appl. Phys.* **1998**, *83*, 7929.
(19) Darakchieva, V.; Paskov, P. P.; Valcheva, E.; Paskova, T.; Monemar, B.; Schubert, M.; Lu, H.; Schaff, W. J. *Appl. Phys. Lett.* **2004**, *84*, 3636.
(20) Klemens, P. G. *Phys. Rev.* **1966**, *148*, 845.
(21) Balkanski, M.; Wallis, R. F.; Haro, E. *Phys. Rev. B* **1983**, *28*, 1928.
(22) Menéndez, J.; Cardona, M. *Phys. Rev. B* **1984**, *29*, 2051.
(23) Ramkumar, C.; Jain, K. P.; Abbi, S. C. *Phys. Rev. B* **1996**, *53*, 13672.
(24) Viera, G.; Huet, S.; Boufendi, L. *J. Appl. Phys.* **2001**, *90*, 4175.
(25) Burke, H. H.; Herman, I. P. *Phys. Rev. B* **1993**, *48*, *15016*.
(26) Gasanly, N. M.; Pala, R. *Phys. Status Solidi B* **2002**, *234*, 665.
(27) Jiménez, J.; Martín, E.; Torres, A.; Landesman, J. P. *Phys. Rev. B* **1998**, *58*, 10463.
(28) Debernardi, A. *Solid State Commun.* **2000**, *113*, 1.
(29) Debernardi, A.; Cardona, M. *Phys. B* **1999**, *263/264*, 687.
(30) Lang, G.; Karch, K.; Schmitt, M.; Pavone, P.; Mayer, A. P.; Wehner, R. K.; Strauch, D. *Phys. Rev. B* **1999**, *59*, 6182.
(31) Sun, C. Q.; Pan, L. K.; Li, C. M.; Li, S. *Phys. Rev. B* **2005**, *72*, 134301.
(32) Pan, L. K.; Sun, C. Q.; Li, C. M. *J. Phys. Chem. B* **2004**, *108*, 3404.
(33) Sun, C. Q. *Prog. Solid State Chem.* **2007**, *35*, 1.
(34) Zhao, M.; Zheng, W.; Li, J.; Wen, Z.; Gu, M.; Sun, C. Q. *Phys. Rev. B* **2007**, *75*, 085427.
(35) Gu, M. X.; Sun, C. Q.; Chen, Z.; Au Yueng, T. C.; Li, S.; Tan, C. M.; Nosilk, V. *Phys. Rev. B* **2007**, *75*, 125403.
(36) Slack, G. A.; Bartram, S. F. *J. Appl. Phys.* **1975**, *46*, 89.
(37) Sheleg, A. U.; Savastenko, V. A. *Vestsi Akad. Navuk BSSR, Ser. Fiz.-Mat. Navuk* **1976**, *3*, 126.
(38) Han, W. G.; Zhang, C. T. *J. Phys.*: *Condens. Matter* **1991**, *3*, *27*.
(39) Cardona, M.; Thewalt, M. L. W. *Rev. Mod. Phys.* **2005**, *77*, 1173.
(40) Reeber, R. R.; Wang, K. *J. Mater. Res.* **2000**, *15*, 40.